International Journal of Automotive Technology, Vol. 5, No. 4, pp. 221–238 (2004)

1229–9138/2004/018–01

VISUALIZATION AND MEASUREMENT OF A NARROW-CONE DI GASOLINE SPRAY FOR THE IMPINGEMENT ANALYSIS

J. S. PARK, K.-S. IM[1)*], H. S. KIM and M.-C. LAI

Mechanical Engineering Dept. Wayne State University,
5050 Anthony Wayne Drive Detroit, Michigan 48202, U.S.A.

(Received 19 September 2003; Revised 28 May 2004)

ABSTRACT–Wall interactions of direct injection spray were investigated using laser-sheet imaging, shadowgraphy, wetted footprint and phase Doppler interferometry techniques. A narrow-cone high-pressure swirl injector is used to inject iso-octane fuel onto a plate, which has three different impact angles inside a pressurized chamber. Heated air and plate conditions were compared with unheated cases. Injection interval was also varied in the heated case to compare dry- and wet- wall impingement behaviors. High-speed macroscopic Mie-scattering images showed that presence of wall and air temperature has only minor effect on the bulk spray structure and penetration speed for the narrow-cone injector tested. The overall bulk motions of the spray plume and its spatial position at a given time are basically unaffected until a few millimeters before impacting the wall. The surface properties of the impact surface, such as the temperature, the presence of a preexisting liquid film also have a small effect on the amount of wetting or the wetted footprint; however, they have strong influence on what occurs just after impact or after a film is formed. The shadowgraph in particular shows that the plate temperature has a significant effect on vapor phase propagation. Generally, 10–20% faster horizontal vapor phase propagation is observed along the wall at elevated temperature condition. For impingement onto a preexisting film, more splash and evaporation were also observed. Contrary to some preconceptions, there is no significant splashing and droplet rebounding from surfaces that are interposed in the path of the DI gasoline spray, especially for the oblique impact angle cases. There also appears to be a dense spray front consists of large sac spray droplets in the oblique impact angle cases. The bulk of the spray is not impacted on the surface, but rather is deflected by it The microscopic details as depicted by phase Doppler measurements show that the outcome of the droplet impaction events can be significantly influenced. Only droplets at the spray front have high enough Weber numbers for wall impact to wet, splash or rebound. Using the sign of vertical velocity, the time-resolved downward droplets and upward droplets are compared. The Weber number of upward moving droplets, which seldom exceeds unity, also decreases as the impact angle decreases, as the droplets tend to impact less and move along the wall in the deflected spray plume.

KEY WORDS : Impingement, Direct injection, Visualization, Shadowgraphy

NOMENCLATURE

m	: dynamic viscosity
r	: liquid density
s	: liquid surface tension
a	: spray cone angle
q	: impact angle. Shown in number only in some figures
δ_{non}	: non-dimensional film thickness
(x, y)	: visualization or measurement point in x and y direction in mm
A	: ambient air (23±2°C) and/or plate temperature (23±2°C) Conditions
DI	: direct injection
DISI	: direct injection spark ignition
GDI	: gasoline direct injection. same term as DISI
H	: H for Elevated air (95±5°C) and/or plate temperature (170±10°C) Conditions
La	: Laplace number
n	: number of droplets; subscript 1 denotes for pre-impingement droplets, 2 denotes for post-impingement droplets
P	: pressure; subscript a denotes ambient, i denotes injection
PDI	: phase doppler interferometer
PFI	: port fuel injection
PMAS	: particle motion analysis system
Re	: Reynolds number
SOI	: start of ignition
t	: time; subscript d denotes duration, i or Δ denote interval, number denotes the frame order in pictures,

**Corresponding author.* e-mail: ksim@wayne.edu

T : ambient temperature; subscript a denotes ambient, w denotes wall
$UBHC$: un-burned hydro carbon
W : wet surface condition
We : Weber number; subscript 1 denotes for pre-impingement droplets, 2 denotes for post-impingement droplets
z : impact distance

1. INTRODUCTION

Fuel economy improvement, potentially up to 30%, is the main driving force behind the recent research and development push toward direct injection spark-ignition (DISI) engines by automotive industry. DISI engines also have potential for significantly improved drivability (transient response, power performance), downsizing benefits, cold start emissions over port fuel injection (PFI) engines. Although complexity in combustion and emissions control, excessive light-load UBHC and high-load NO_x emissions are among their main drawbacks (Zhao *et al.*, 1997, 1999). In order to maximize DISI performance, fuel system needs to successfully adapt at least two distinct operating modes: the late injection timing during the compression stroke for the stratified-charge mode at part-load, and the early injection timing homogeneous-charge mode during the intake stroke at high load.

The impingement of liquid fuel on the combustion chamber wall and piston head is generally undesirable in IC engines because it increases UBHC emissions and affects the combustion phasing during acceleration transients (Yoo *et al.*, 1998; Stanglmaier *et al.*, 1999; Li *et al.*, 1999). Fuel films that exist during combustion of the premixed charge ignite to create piston-top pool fires. These fires and the soot particles produced inside the combustion chamber have been characterized using direct flame imaging and found to persist throughout the exhaust stroke, implying that piston-top pool fires are a likely source of engine-out particulate emissions for DISI engines (Stevens *et al.*, 2001). It is obvious that the mass, thickness, shape and time-history of any fuel wetted area in the engine, whether the wetting is intentional or unintentional, are parameters that can influence combustion and emissions. On the other hand, in wall-guided stratified charged combustion mode, the impingement of gasoline spray on the piston wall is intended in order to divert the rich mixture to spark plug for successful ignition and stable combustion. In this case, the piston wall or cavity is used to guide the fuel/air mixture flow toward a spark plug along the cavity wall by the penetrating force of the fuel spray. The spray is assisted only slightly by either the swirl or tumble motion of the intake charge (Wirth *et al.*, 1998) in the wall-guided systems.

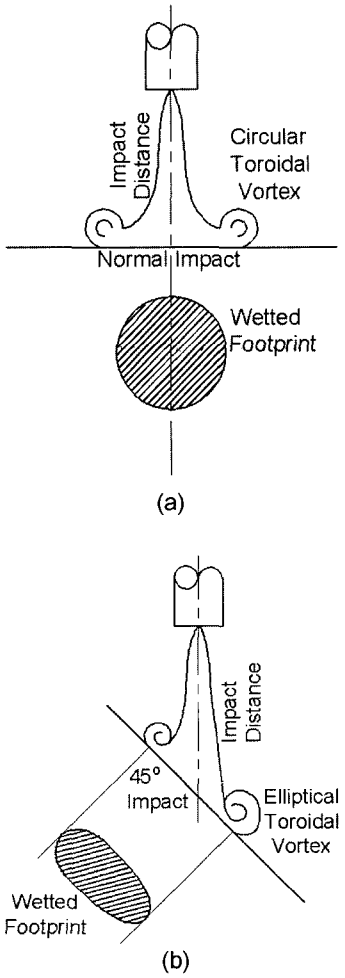

Figure 1. Spray-wall interactions for a narrow-cone swirl-type DI gasoline injector at the impact angle of (a) 90°, and (b) 45°.

As shown in Figure 1, the complexity of spray-wall interactions can be demonstrated by the number of parameters involved. A multi-phase spray can be defined by its cone angle or shape, injection parameters (pressure, duration), fuel properties, and ambient conditions. The wall can be defined by its impact distance, angle, curvature, temperature, roughness, and the presence of deposits or pre-existing liquid film. In addition, the interaction of liquid droplets with solid surfaces can result in enhanced wall atomization, heat transfer between the liquid and the surface and the formation of liquid films (Senecal *et al.*, 1998). Tens of parameters are influential in the overall process that incorporates the aerodynamic and liquid-vapor-solid interactions process, which is the reason why this is a very difficult area to correlate and model.

An impinging droplet undergoes many different

conditions depending on the pre-impingement droplet conditions. Although the mechanism is different from one study to another, it can be summarized as follows;

a. Stick: Impinging droplet adheres to the wall. This occurs when the impact energy is very low and the wall temperature is relatively low.
b. Spread: Impinging droplet impacts with a moderate velocity onto a wall and spreads out to form a wall film or merges with the pre-existing liquid film.
c. Rebound: Impinging droplet bounces off the wall after impact.
d. Break-up: Droplet first undergoes a large deformation to form a radial film on the surface, then the instability within the film causes the fragmentation of the liquid film in a random manner.
e. Splash: Following the collision of a droplet with a surface at very high impact energy, a crown is formed, jets develop on the periphery of the crown and the jets become unstable and break up into many fragments.

While a droplet undergoes the above one or combination of multiple mechanisms, the fuel film formed also interacts with pre-impingement droplets, air flow, and the wall. Fuel film movement is also possible as a result of the combined effects of droplet momentum, shear force by air, and the wall shear force. Whether a drop forms a

Table 1. Summary of impingement regimes and criteria in simulation models.

Author	Impingement regime & Conditions			
	Dry Wall		Wet Wall	
	Regime	Condition	Regime	Condition
Habchi *et al.* (1999)	Stick Rebound Spread Splash	N/A N/A $We = \frac{(57.7)^2}{Re}$	Stick	$We = 18^2 d_o \sqrt{\left(\frac{\rho}{\sigma}\right)} \sqrt[4]{\left(\frac{\mu}{\rho}\right)} f^{3/4}$
Bai & Gosman (1995)	Adhesion Splash	$We = A \cdot La^{-0.18}$	Rebound Spread Spread Splash	$We \cong 5$ $We \cong 1320 \cdot La^{-0.18}$
Han *et al.* (2000)	Stick Rebound Spread Splash	N/A N/A N/A $We_n Re_n^{0.5} \geq H_{cr} = \left(1500 + \frac{650}{Re}\right)[1 + 0.1 Re_n^{0.5} \min(\delta, 0.5)]$	Stic Rebound Spread	$We < t$ $5 < We < 10$ $We > 10$ and $We_n Re_n^{0.5} < H_{cr}$
Mundo *et al.* (1994)	Stick Splashing	$Oh \cdot Re^{1.25} = 57$	N/A	
Stanton & Rutland (1996)	Stick Rebound Spread Splash	$T_w < T_{pa}$, $We < 5$ $5 < We < 10$ $We = 18^2 d_o \sqrt{\left(\frac{\rho}{\sigma}\right)} \sqrt[4]{\left(\frac{\mu}{\rho}\right)} f^{3/4}$		
Nagaoka *et al.* (1994)	Stck Non-stick	$We = 80$		
Naber & Reitz (1988)	Stick Reflect Jet	Lew We Moderate We $We \cong 40$		
Senda *et al.* (1999)	Stick Splash	$We = (2164 + 7560 \cdot \delta_{non}^{1.78}) \cdot La^{0.2}$		

Note: f is splashing threshold defined as V_{nd}/d_d, where V_{nd} is normal velocity and d_d is diameter of droplet. δ_{non} is a non-dimensional film thickness defined as δ_{fl}/δ_{in}. where δ_{fl} is film thickness and d_{in} is impinging droplet diameter.

film, enters a film, rebounds intact, shatters and rebounds or splashes within a film is primarily determined by the Weber number of the drop and the angle of approach, and influenced by the surface properties. The importance of Weber number in the drop impact processes can be demonstrated in Table 1, which is a summary of previous modeling investigations of the spray-wall interactions. There is not yet an agreement regarding the proper Weber number thresholds for different regimes. The researches in past have mostly focused on the spray impingement in diesel engines (e.g., Nishida *et al.*, 1990; Zulo *et al.*, 1991) and more recently PFI engines (Senda *et al.*, 1999) but there are very few experimental data on high-pressure gasoline spray wall interactions.

As commonly known, gasoline has numerous different properties from diesel fuel such as lubricity and octane number. The fuel pressures that have been selected for most of the current prototype DISI engines range from 2 to 12 MPa, which are quite low when compared with diesel injection systems of 40 to 200 MPa, but are relatively high in comparison with typical PFI injection pressures of 0.25 to 0.5 MPa (Zhao *et al.*, 1995). The spray structure is also quite different depending on whether a swirl, slit, multi-hole or air-assist injector is used. Previous results and correlation on a single droplet impingement may need to be modified in light of the multiple droplet effects and aerodynamic interactions with solid wall. Thus, the spray impingement in DISI engines must be studied in its own class to more fully understand these complex processes. In addition, there are very few DISI impingement experimental data available to validate the computational fluid dynamics (CFD) sub-models, which is increasingly needed to aid engine design.

High-speed microscopic visualization and PIV techniques were used to study the DISI gasoline spray-wall interactions and show clearly the film build-up and vaporization at both ambient and elevated temperature, especially for narrow cone spray (Park *et al.*, 1999). Droplet rebounding and film break-up are clearly observed. Post-impingement droplets are significantly smaller than pre-impingement droplets with a more horizontal velocity component regardless of the wall temperature and impact angle conditions. In this study more results of the narrow-cone injector wall impingement processes are reported. Iso-octane replaced gasoline as the test fuel to simplify CFD comparison in the future. The chamber pressure is also increased to focus on high compression ratio or turbo-charged DISI applications. More detailed phase Doppler data and impingement wetted footprint data are reported.

2. EXPERIMENTAL SETUP

The experimental setup includes a DISI injection system, a heated impingement plate, pressurized chamber, and air flow control. Three optical systems were used for visualization and measurement: high-speed macroscopic visualization, shadowgraphy, and phase Doppler interferometer (PDI) system. The injection system consists of a fuel tank pressurized by a nitrogen gas cylinder, an injection driver, and a high-pressure narrow-cone with a nominal cone angle α=20°. A PC controls the injection timing, the injection duration, and the external time signal to the measurement systems. To simplify the experiment, the injection pressure and duration are kept at 6.8 MPa (1000 psig) simulating the late injection stratified charge mode. The duration is kept short at 0.5 ms to minimize optical obscuration in dense-spray upon impingement during visualization and measurements. The short injection creates slightly larger dropsize due to injector pintle opening and closing transients, similar to previous study (Park *et al.*, 1999). Two time separations between repeated injections: 3 and 0.3 second for ambient temperature conditions, and 1 and 0.1 second for elevated temperature conditions, are chosen to simulate a dry and a wet (i.e. with pre-existing fuel film) surface conditions respectively. Fuel is injected 7 times prior to taking a shadowgraph to wet the surface for ambient and elevated temperature conditions. Iso-octane is used as a single compound fuel to simplify future CFD analysis.

The basic experimental set-up is shown in Figure 2. The pressurized chamber has three large optically accessible windows for measurements and visualizations, and the pressure inside the chamber is kept at 0.470 MPa (absolute) throughout the experiment. The airflow control system consists of a compressor, air accumulator, air flow

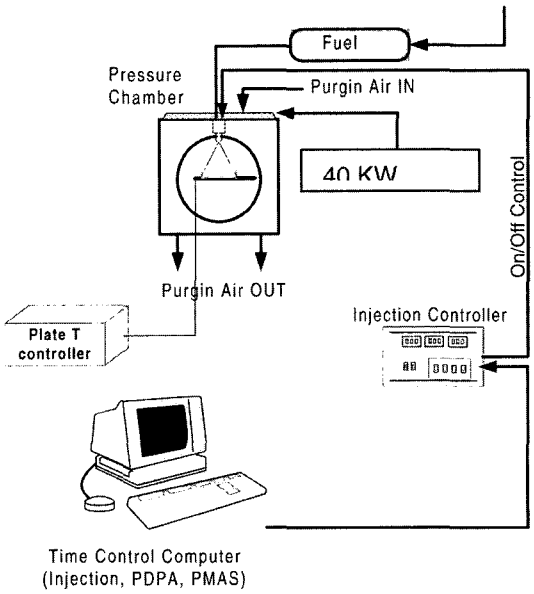

Figure 2. Basic experimental set-up.

and pressure regulators, and a 40 kW heater. Purging air, either at ambient or elevated temperatures, flows slowly from the top of the chamber, heated by a 40 kW heater upstream and exits at the bottom of the chamber. One thermocouple is placed above the plate to monitor the air temperature of the spray-passing zone.

A 13 mm thick aluminum plate is heated from below with a thin etched-foil heater attached on the back. One thermal ribbon checks the temperature of the plate and sends the temperature information to a feed-back controller outside the chamber. The aluminum plate is located 38 mm directly below the injector tip, and can be tilted to various impact angles, which in this experiment is adjusted to three different angles (q=45°, 60°, and 90°). Different air and the plate temperatures are chosen for the test conditions: For the cold start conditions, the temperature of the air and the plate is about the same as the ambient temperature; i.e., T_a=T_w=23±2°C. For elevated temperature conditions, the air is kept at T_a=95±5°C and the plate is kept at T_w=170±10°C.

High-speed pulsed laser-sheet is used to observe the overall liquid phase spray structure using Mie scattering. The optical diagnostic systems include a copper-vapor laser (Oxford Laser 15U) and a high-speed 35 mm drum camera as imager. The copper-vapor laser beam is expanded into a thin sheet using cylindrical lens and is used as an optical shutter, up to 10 kHz. Shadowgraph technique is used to visualize the liquid and vapor phase spray plume propagation using a Particle Motion Analysis System (PMAS from Vtek). PMAS consists of a macroscopic lens, a CCD camera, and an ultra fast high-energy electric discharge capable to generate a 50-ns spark with an energy output of about 1.5 Joules. A PC controls the timing of the spark discharge, image acquisition of the camera and image processing. The

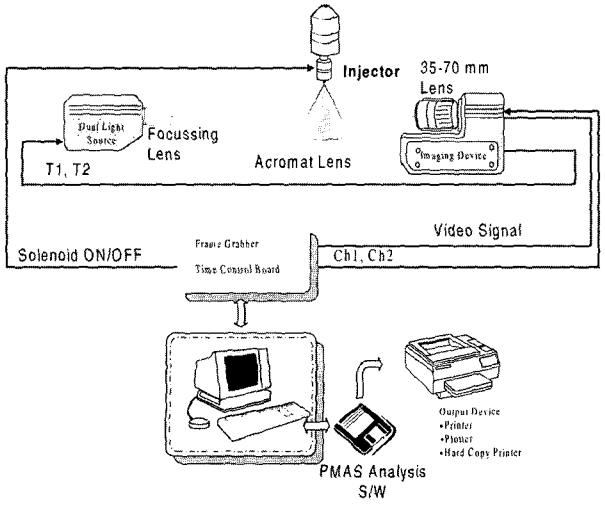

Figure 3. Shadowgraph set-up.

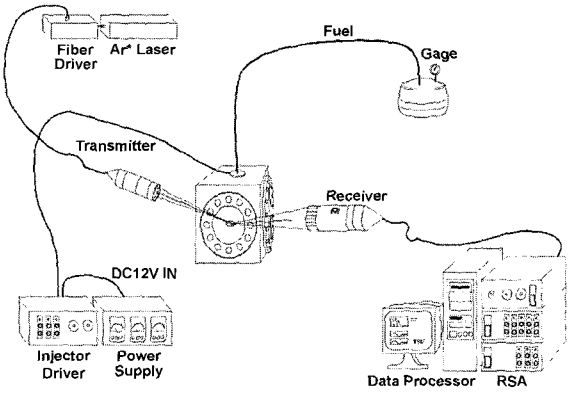

Figure 4. PDI set-up.

PMAS set-up is shown in Figure 3.

A two-channel phase Doppler Interferometer (PDI) with a 1-Watt Argon-ion laser is used to measure droplet size and velocity of the spray. PDI measurement in high pressure conditions is more difficult than those in ambient pressure conditions. Four laser beams (two blue beams in horizontal arrangement and two green beams in vertical arrangement) go through the transparent window of the spray chamber. The PDI set-up is shown in Figure 4.

Figure 5 shows the measurement locations with respect to the wall and wetted footprint of the injection. 5000 samples are collected at each measurement location. Usually two layers of measurement points are chosen to observe the droplet behaviors in the vicinity of the impingement area, up to 1mm vertical distance from the wall and 2 mm above the lower layer of the measurement points. Wetted footprint is obtained using special papers which change its colors when in contact with liquid fuel. Details of the footprint experimental procedure and discussions can be found in later part of this paper.

Based on the PDI measurements, the Weber number of the droplets, is calculated and grouped into two groups according to the direction of the vertical components. Those having vertically downward direction are denoted as group 1 and those in the upward direction as group 2. Group 2 droplets are not necessarily rebounded or splashed from surface, but because they are measured very close to the wall surface, the chances of them being post-impingement droplets are very high. The experimental conditions are summarized in Table 2.

In order to simplify the notation in the Figure captions, the following naming system will be used to designate test conditions:

$$\mathbf{T}\ \theta\ (\mathbf{x},\ \mathbf{y})$$

where **T** = A for Ambient air (23±2°C) and
plate temperature (23±2°C), or

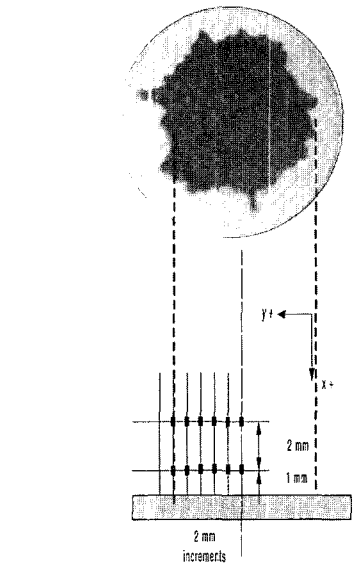

(a)

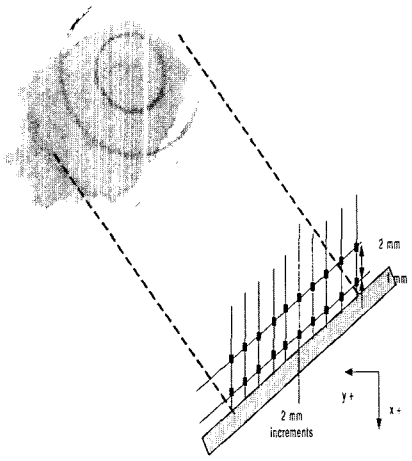

(b)

Figure 5. PDI Measurement locations with respect to wall and impingement wetted footprint: (a) Top: θ = 90° (b) Bottom: θ = 60°.

T = H for Elevated air (95±5°C) and plate temperature (170±10°C),
$\boldsymbol{\theta}$ = Impact angle (90°, 60°, or 45°), and
(x, y) is the PDI measurement location, where x is the horizontal distance from the wall, and y is the vertical distance from the spray axis

Surface condition is dry for the cases shown in this paper unless otherwise noted; i.e., an appended **D** or **W** denote dry or wet surface condition. For example:

A 90 (0, 1)

Table 2. Experimental conditions

	Category	Values
Ambient air	T_a (°C)	23±2 for ambient conditions 95±5 for elevated conditions
	P_a (kPa)	470 kPa (absolute)
Injection	Fuel	Iso-octane (C_8H_{18})
	Injector	α=20° Swirl DISI injector
	P_i (MPa)	6.8
	t_d (ms) (duration)	0.5 (injection duration)
	t_i (ms) (interval)	3000 for dry, 300 for wet at amb. 1000 for dry, 100 for wet at elev.
Plate	T_w (°C)	23±2 for ambient conditions 170±5 for elevated conditions
	Impact distance	Z=38 mm below the injector tip
	Impact angle (θ)	45°, 60°, 90°

designates ambient air and plate temperature, 90° impact angle, and measured at (0, 1) location and dry wall conditions.

3. RESULT AND DISCUSSIONS

3.1. High-speed Laser Light-sheet Visualization

Results of the macroscopic visualization using high-speed pulsed laser light sheet and drum camera are shown in Figure 6. Only ones in every five frames are shown for brevity. The first frame is taken at 0.4 ms after SOI, and the time interval thereafter is 0.5 ms. All impingement images shown in the Figure are taken at dry surface conditions, since those for the wet surface conditions do not have significant difference. The ambient case is shown first and is immediately followed by the heated case for comparison. Different impact-angle cases are shown in the order of decreasing impact angle; i.e., Figures 6a and 6b are for 90 degree impingement, 6c and 6d are for 60 degree impingement, and 6e and 6f are for 45 degree impingement. Figures 6a, 6c, and 6e are the impingement at ambient temperature conditions, while 6b, 6d, and 6f are the impingement at elevated temperature conditions.

Due to the dense narrow cone spray structure, the toroidal vortex is not as obvious as in the wider cone (Park *et al.*, 1999). Therefore, the spray impingement process is similar to that of the PFI and diesel wall impingement process, although the dropsize and spray momentum are quite different. Secondary injection due to needle buncing is obvious in the image taken at 1.4 ms after SOI. Fuel film formed on the impinging surface is

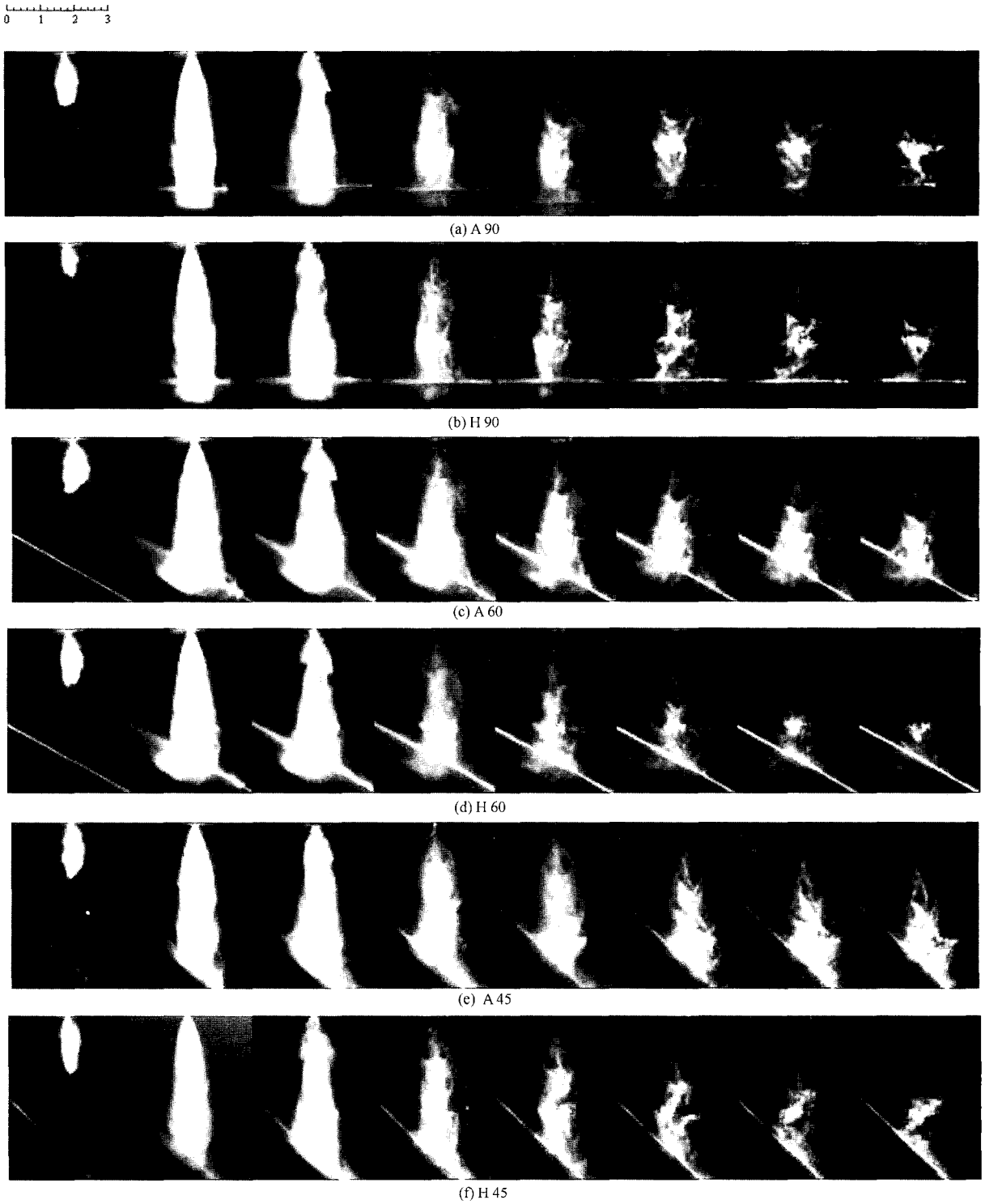

Figure 6. High-speed laser light-sheet Mie scattering visualization (t_l=0.4 ms, Δt=0.5 ms).

visible, but the film resolution is not fine enough to evaluate the thickness. The elevated temperature conditions show more skeletal spray structures due to faster fuel evaporation, especially at the later stage of the visualization. Observation of the spray structure shows that the spray penetration speed is almost identical in all cases. Spray

width at elevated temperature condition is slightly less than the spray width at ambient temperature condition for all three different impact angles due to the evaporation of fine droplets at the edge of the spray. Edge detecting analysis performed in some of macroscopic images shows that the spray width changes slightly by approximately 10%. It takes approximately 1ms for the spray front to reach the wall surface. The earliest droplets that arrive are the least influenced by the entrainment airflow field, as this field is just being established. They are generally also the largest and fastest drops, as was clearly demonstrated in the later time-resolved droplet arrival measurements.

3.2. Shadowgraph Visualization

Results of the shadowgraph visualization are shown in Figure 7. The dimension of the viewing area is 45 × 30 mm (W × H). Dark horizontal section at the bottom of the images is the impingement wall surface. It is more difficult to distinguish it for the wet surface at elevated temperature conditions due to active evaporation of the fuel; however, it can be easily calibrated in advance. Another dark section at the upper left corner of the image is due to the chamber geometry. Figure 7a and 7c show the comparison between dry and wet surface impingements. For dry surface case, the evaporation occurs upon the impingement, while the evaporation is already in

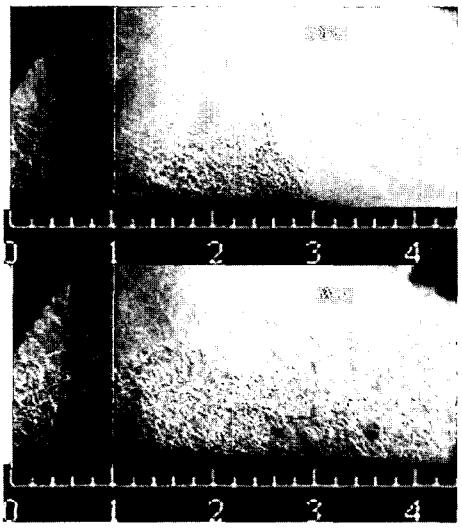

(a) Surface effect: **H 90 Dry** (top), **H 90 Wet** (bottom), t=2.5 ms

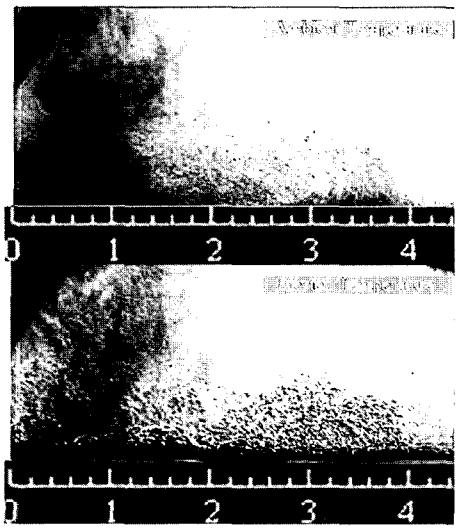

(b) Temperature effect: **A 90** (top), **H 90** (bottom), t=3.5 ms

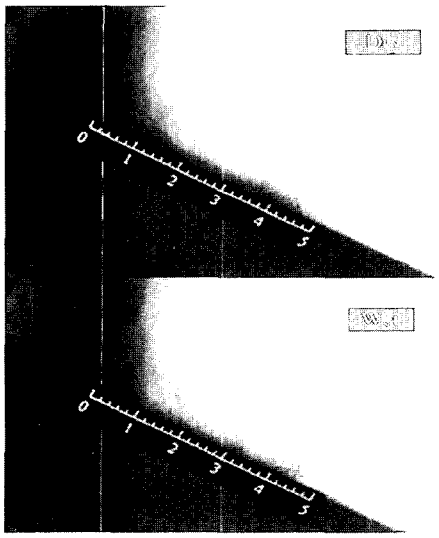

(c) Surface effect: **A 60 Dry** (top), **A 60 Wet** (bottom), t=1.5ms

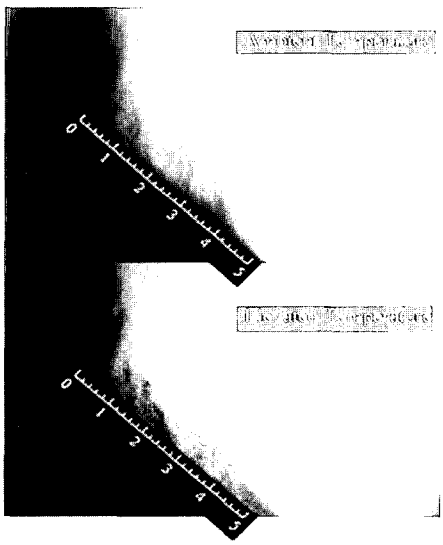

(d) Temperature effect: **A 45 W** (top), **H 45 W** (bottom), t=1.5ms

Figure 7. Shadowgraph visualization.

progress from the existing fuel film for the wet surface case. More evaporation is observed in wet surface impingement. Quantitative analysis of the vapor propagation is not attempted since active fuel evaporation near the surface prevents clear visualization.

Figure 7(b) and 7(d) shows the temperature effect on the vapor phase propagation. Image taken at elevated temperature condition obviously reflects more active evaporation than that at ambient temperature condition. Horizontal vapor propagation at elevated temperature conditions is about 10~20% faster along the wall as shown in the Figure, while vertical vapor propagation does not change significantly. The reason for the similarity in vertical vapor phase propagation is due to the stagnation flowfield set up by the impingement fuel spray from the injector.

Figure 8 shows the vapor phase propagation according to various impact angles. Images are processed to better visualize the vapor phase. Vertical vapor propagation is about the same for all impingement cases, while horizontal vapor propagation becomes longer as the impact angle decreases. While the higher angle impingement promotes the evaporation vertically, the lower angle impingement promotes the spray plume to slide along the surface, resulting in longer horizontal vapor propagation as shown in Figure. This shows that there is not significant splashing and droplet rebounding from surfaces that are interposed in the path of the DI gasoline spray, especially for the oblique impact angle cases. There also appears to be a dense spray front consists of large spray droplets in the oblique impact angle cases.

The bulk of the spray is not impacted on the surface, but rather is deflected by it. The misconception that there should be very significant splashing and droplet rebounding in DI gasoline spray maybe originated from the single-droplet experiments in which there is no spray-induced flowfield. This misconception is enhanced by the fact that PFI fuel spray tests do generally indicate splashing and rebounding, particularly for PFI fuel sprays that impact a pre-existing liquid puddle. This viewpoint may at first seem logical from the very elevated fuel rail pressures that are used in DISI engines; however, these fuel pressures produce very small drops having high drag, rapid vaporization rates and enhanced momentum transfer to the surrounding air. Rather than increasing the droplet impact rates and splashing, an increase in fuel pressure diminishes it.

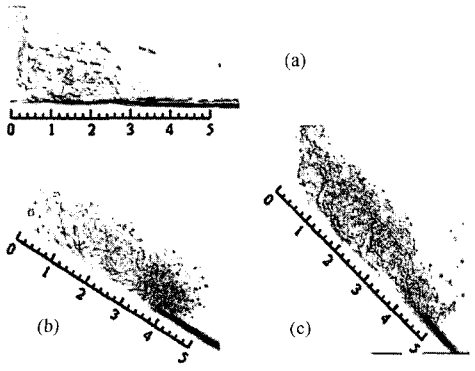

Figure 8. Vapor phase propagation by impact angle; t=1.5 ms. (a) **A 90 W** (b) **A 60 W** (c) **A 45 W**

3.3. Wetted Footprints

Prior to show the PDI measurement results, understanding the change of wetted footprint according to the impingement parameters. The wetted footprint of a DISI fuel spray is a key metric for a combustion system development program, as it is an indicator of spray targeting. It has also been related to the piston-top pool fires and engine-out soot emissions (Stevens *et al.*, 2001). Only the spray droplets that have sufficient momentum when nearing and interposed surface will impact that surface.

The visualization of wetted footprint is carried out inside the pressurized chamber using a 35-mm SLR film camera. A special paper used for practicing calligraphy, as it changes color when wetted, is placed on top of the target plate to record the wetted footprint at different time after SOI. Although the calligraphy paper changes the surface characteristic of the aluminum plate, it still provides important fundamental information on how the fuel film changes with respect to various parameters. Typical wetted Images are shown in Figure 9. Because there are injection-to-injection variations, three selected cases are shown to demonstrate the variation, which is not significant.

Under the unheated conditions shown in Figure 9a–9c, the evaporation of the absorbed fuel off the paper is slow inside the pressurized chamber, so that the variation according to the time elapsed is not significant up to 10 ms after SOI. However, under heated air and plate conditions, it is critical to take the wetted footprint as soon as the injection is completed. As expected, decreasing impact angle results in longer and slimmer wetted footprint as shown in Table 3. As the impact angle decreases, spray plumes are more likely to be deflected than to impinge on it. The reduced width of the wetted footprints at oblique impact angle cases show that there is

Table 3. Wetting region variation.

	$\theta = 90°$	$\theta = 60°$	$\theta = 45°$
Length	22	25	30
Width	22	20	15

Unit : (mm)

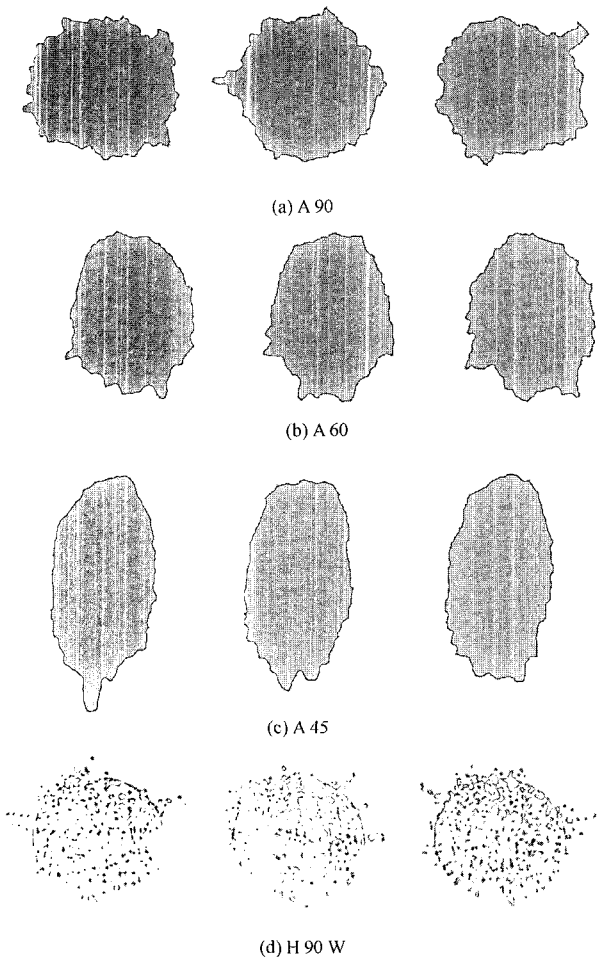

(a) A 90

(b) A 60

(c) A 45

(d) H 90 W

Figure 9. Wetted footprints: unheated cases at different impact angles: (a) 90°, (b) 60°, (c) 45°, and (d) heated case at 90°.

significant variation in liquid fuel film formation and movement with respect to impingement angle in the unheated cases. However, the radial film spread of the film is driven by the impinging spray-plume and converted more to the down-hill direction as the impact angle decreases.

The heated cases shown in Figure 9(d) were taken at 2 ms after SOI at higher injection rate. Only a few large sac spray droplets are visible due to the short injection duration.

4. PDI MEASUREMENT

Figure 10 PDI results of free spray (a) at atmospheric and (b) at pressurized ambient conditions, and the impinging spray (c) at pressurized condition.

In order to check the difference in the PDI results between the free spray and the impinging spray,

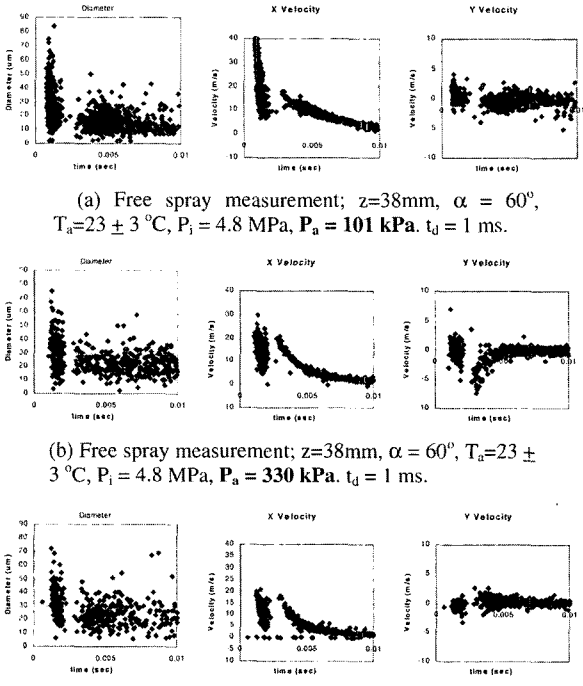

(a) Free spray measurement; z=38mm, α = 60°, T_a=23 ± 3 °C, P_i = 4.8 MPa, **P_a = 101 kPa**. t_d = 1 ms.

(b) Free spray measurement; z=38mm, α = 60°, T_a=23 ± 3 °C, P_i = 4.8 MPa, **P_a = 330 kPa**. t_d = 1 ms.

(c) Impinging spray measurement; z=38mm, α = 60°, θ = 90°, T_a=23 ± 3 °C, **T_w=95 ± 5 °C**, P_i = 4.8 MPa, P_a = 330 kPa. t_d = 1 ms, **2mm above the plate.**

Figure 10. Timeresolved We_l number measurements.

experiments without and with the plate are performed. A typical result is shown in Figure 10 for a wide-cone angle injector. As shown in the Figure 10, the droplets start to appear about 1 ms after SOI, and after 10 ms, the droplets measured are mostly the airborne droplets from the impingement or following the turbulent flow field. Thus, it is reasonable to only show the measurement data from the beginning of the injection up to 10 ms to eliminate the effects of the airborne droplets.

Figure 10(a) and 10(b) show the free spray results at different pressure conditions. Droplet diameter is slightly smaller at ambient pressure condition, but x-velocity at ambient pressure is significantly higher compare with the case at pressurized condition. This is due to the increase drag force at higher ambient density decreases the spray penetration and droplet velocity. The effect of wall can be characterized microscopically by comparing Figure 10(b) and 10(c). The droplet diameter and velocity distributions are not significantly different at 2 mm away from the wall, as the wall effect is negligible in all spray characteristics at this location. However, due to the wall interactions, the distribution of the normal-velocity in the impingement case is wider than the free spray case. The rebounded droplet can be seen to have small vertical velocity components during main spray impact. The presence of wall also has a more dramatic effect on the

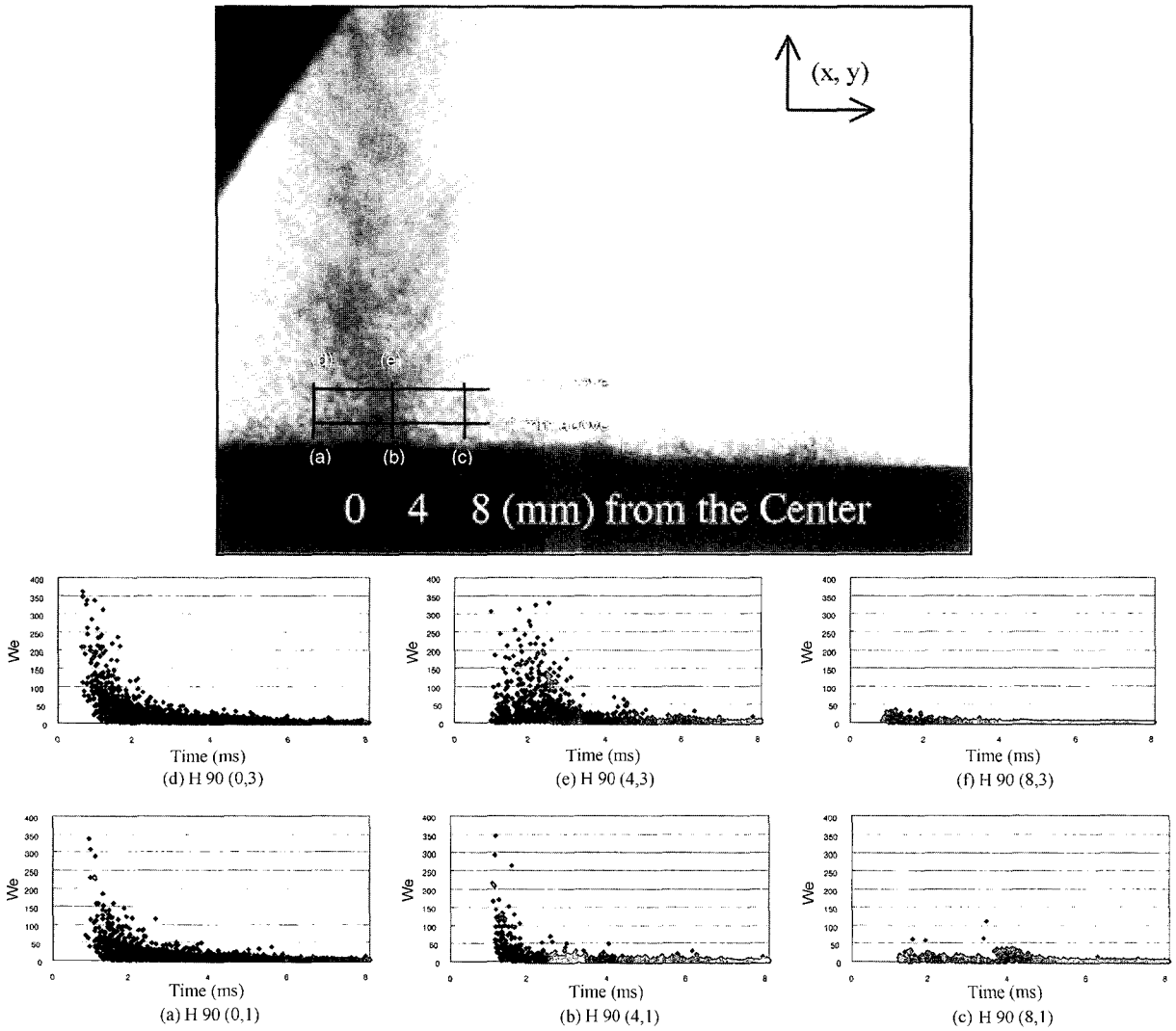

Figure 11. K-value calculation of Figure 11e.

spray tails as it broadens the velocity distribution.

Figure 11 shows the time-resolved Weber number calculations and their measurement locations with respect to the wall and spray axis for 90-degree impact under heated conditions. Most droplets only start to appear approximately after 1 ms. after SOI. This time delay slightly varies according to the measurement location, plate position, and temperature. Droplet diameter ranges from 2 to 50 micrometers, and x-velocity (vertical velocity) ranges 1 to 15 m/s., with the largest and faster droplets presumably from the transient sac spray arriving first. Droplets having positive x-velocity (downward), will be denoted as 1, and droplets having negative x-velocity (upward) will be denoted as 2, regardless of impact angle. Those droplets having negative x-velocity are considered to be either rebounding/splashing droplets or just turning droplets following the upward turbulence flow field.

Figure 11 shows that Weber number generally decreases and loses the characteristic spray front pattern as the measurement location moves further from the center. At location 4 mm from the center, the signature spray front pattern starts to degrade and completely disappeared at 8 mm from the center. Comparing Weber number measured at 1 mm and 3 mm above the plate, Weber number at 3 mm above the plate is slightly higher since droplets further from the stagnation surface retains their higher inertia. In addition, time lag until the droplets are captured in the probe volume is slightly shorter at 3 mm above the plate since it has shorter distance from the injector tip. Overall observation of Figure 11 shows that only a small group of droplets appeared −1 to 2 ms after SOI has large enough momentum to splash. According to Table 1, most droplets after 3 ms will stick to the surface.

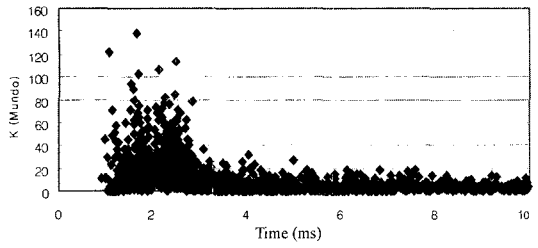

Figure 12. K-value calculation of Figure 11e.

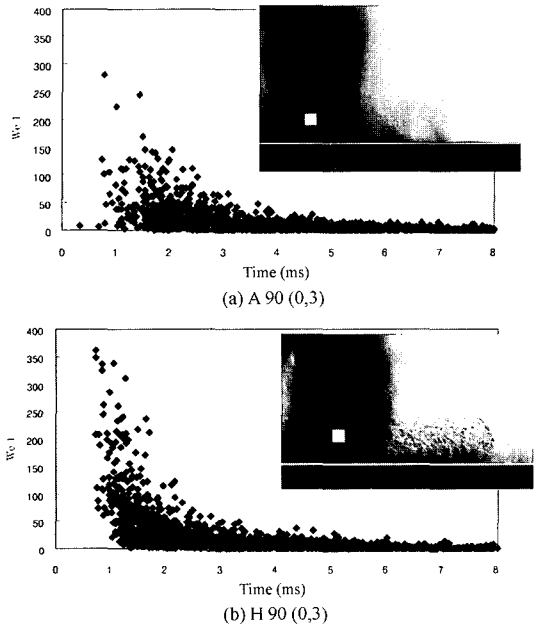

Figure 13. Temperature effect on *We*.

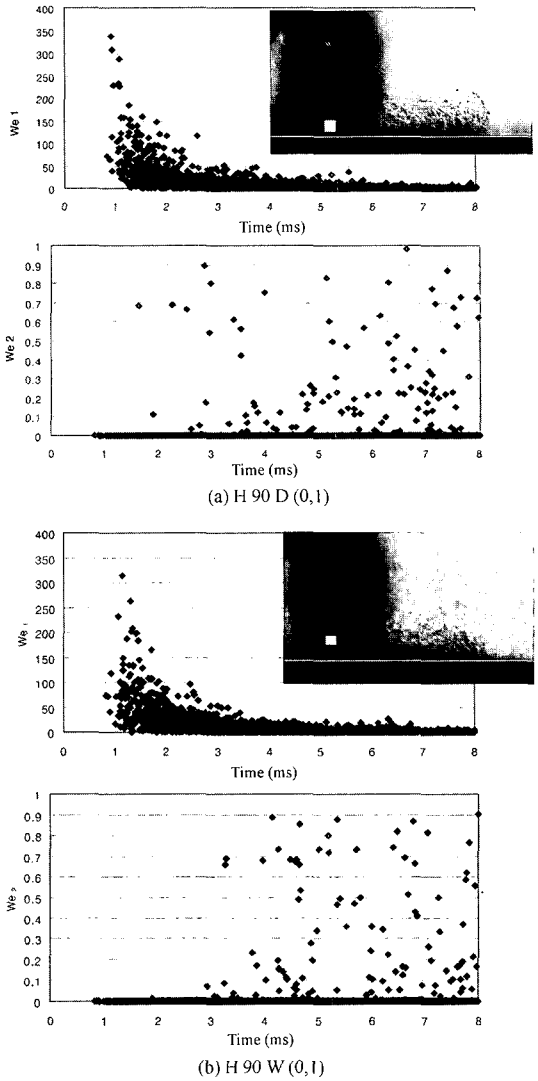

Figure 14. Surface condition effect on *We*.

For example, Figure 12 shows that only small number of droplets having K ($=Oh^{*}Re^{1.25}$) value over 57 or Weber number over 80 will splash (Mundo *et al.*, 1994), with the maximum Weber number capped at 400 for these test cases.

Figure 13 shows the effect of temperature on Weber numbers under 90-degree Impact angle and dry surface conditions. Measurement location is chosen to clearly display the difference. Number of sample is about the same in both Figures, but looks different in the Figure due to the overlap of data points for the first 10 ms after SOI. Spray arrival time displays minor difference, but spray pattern shows significant difference. The spray front is more clearly observed at elevated temperature. It is believed that large droplets in the spray front travels faster in less dense air at elevated temperature. Weber numbers for the droplets having negative vertical velocity component are very close to 0 for both cases and therefore are not shown.

Figure 14 shows the effect of preexisting fuel film on Weber numbers under 90-degree Impact angle and heated conditions. Measurement location is chosen near the surface, at 1mm above the plate. The We_1 and We_2 numbers for both cases display almost identical patterns, which shows that the preexisting fuel film condition as specified in the current test procedures does not significantly affect the wall impingement processes. The hot surface quickly vaporizes the fuel film, whose thickness may not be significant to affect the later spray impingement. Most droplets having upward velocity have near-zero Weber number, as they either belong to re-atomized droplets which are significantly smaller or to the small airborne droplets entrained by the upward turbulent flow eddies. However, the number of upward droplets having significant Weber number is small as only a small portion of the impinging droplets are capable

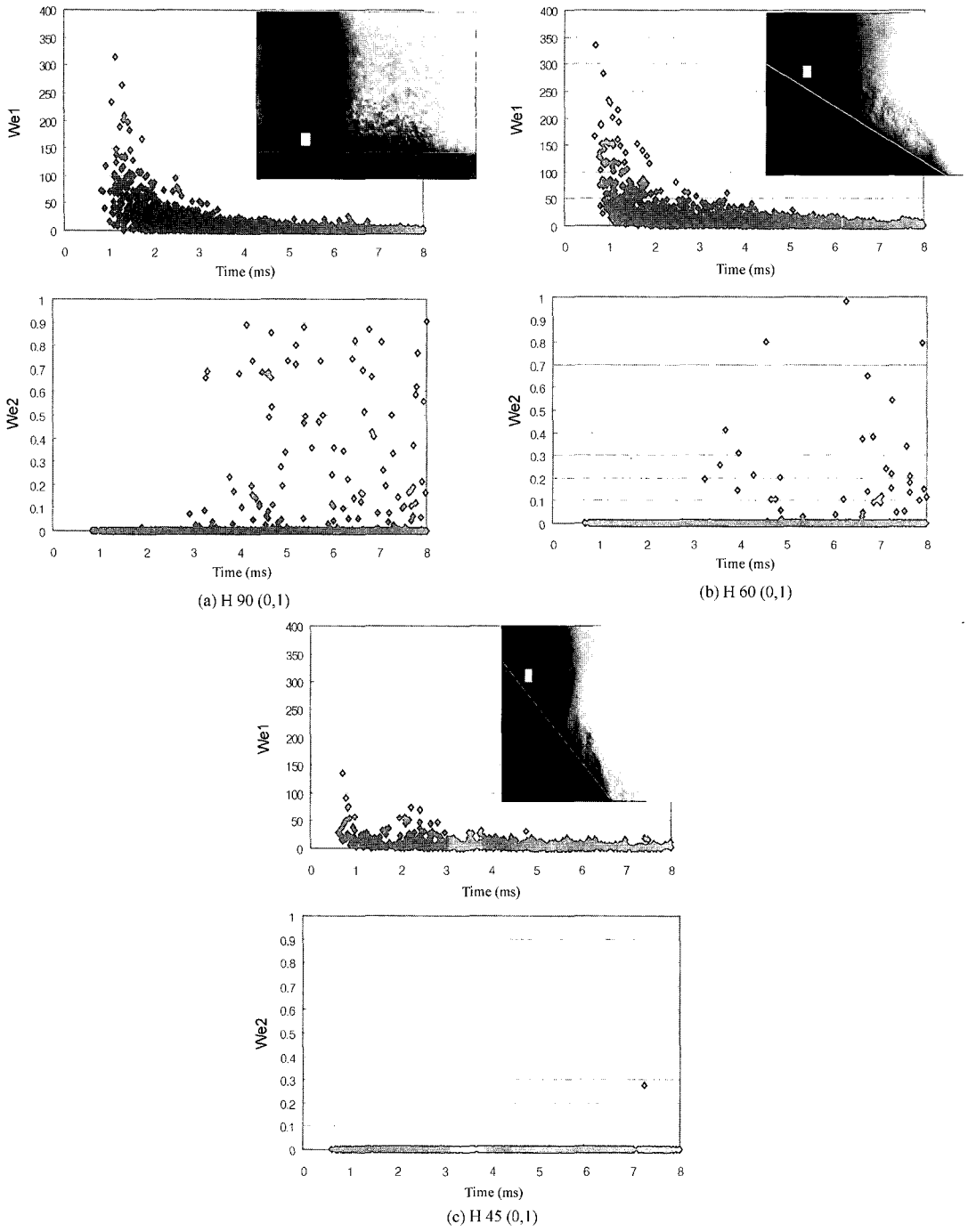

Figure 15. Impact angle effect on *We*.

of splashing. While their Weber numbers are much larger than those of the entrained droplets, they do not exceed the maximum value of unity in the most of the cases tested.

Figure 15 shows the effect of impingement angle on Weber numbers for elevated temperature and wet surface conditions. Droplet arrival time for three impact angles is almost identical; however, droplet Weber numbers decrease significantly for the most oblique impact angle of 45°. This shows that the presence of wall significantly alters the spray flow pattern. As the impact angle decreases, spray plumes are more likely to be deflected than to impinge on it. This observation is also true from We_2: As the impact angle decreases, number of droplets

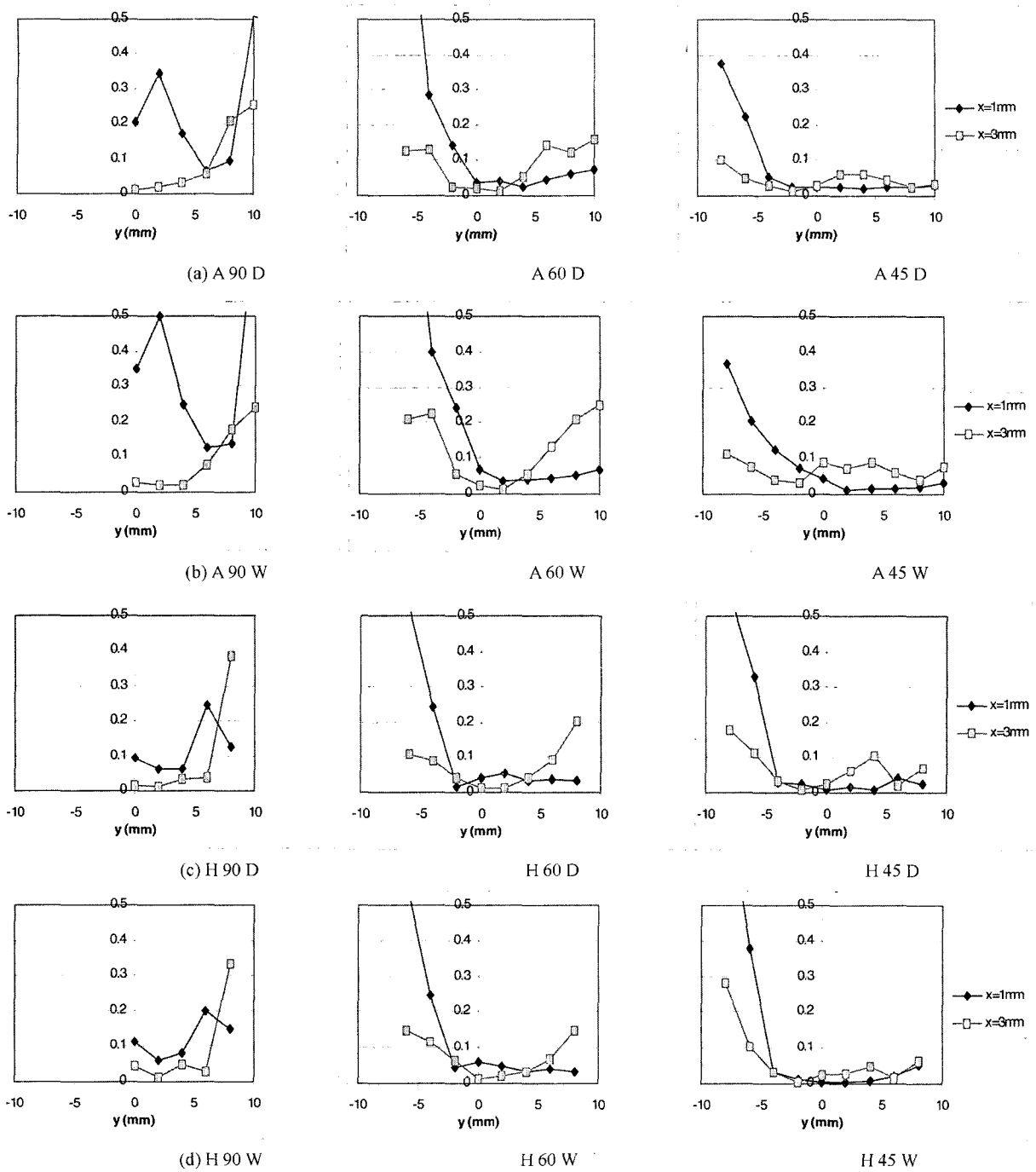

Figure 16. Time averaged PDI results: n_2/n_1.

having significant We_2 also decreases as We_1 decreases. More spray droplets change its direction to follow the airflow along the surface, which is consistent to the findings in the shadowgraph visualization.

Time-averaged PDI data, from 0 to 15 ms after SOI, are shown in Figures 16, 17, and 18. Droplets after 15 ms after the injection are considered to be the airborne droplets, which do not have any initial momentum from the injection, thus excluded from the time-averaged data. The dry and wet surface cases show very similar time-averaged behaviors, showing good repeatability of the measurement data and consistent with findings in the time-resolved measurements.

Figure 16 shows the rebound ratio n_2/n_1 from PDI results,

which is the ratio of the number of upward-bound droplets to that of the downward-bound droplets. Inclusively, it is also indicative of the relative frequency of the rebound and splashed droplets with respect to the pre-impingement droplets. Generally, the ratio is less than 0.5, and the ratio increases as the distance from the wall (x) increases. For unheated normal (q=90°) impingement cases, the ratio changes from a donut-shape profile at 3 mm away from the wall, to a double-peak profile at 1 mm away. This is due to the stagnation flow characteristics and active rebounding at the center of the spray axis.

For oblique (q=60° and 45°) impingement cases, n_2/n_t measured closer to the wall (x=1 mm) is higher in the uphill (negative y) direction because the local impact

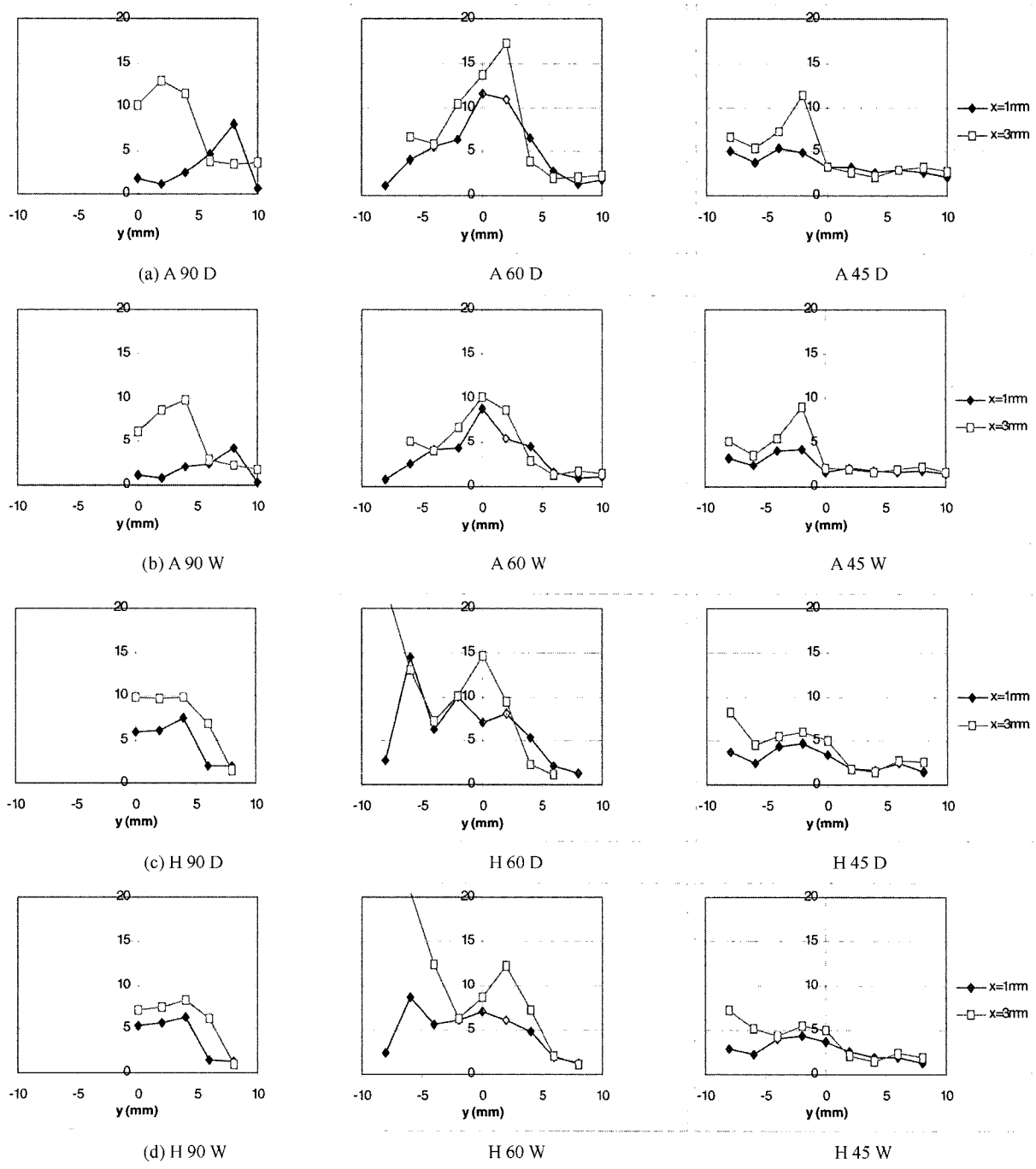

Figure 17. Time averaged PDI results: *We*.

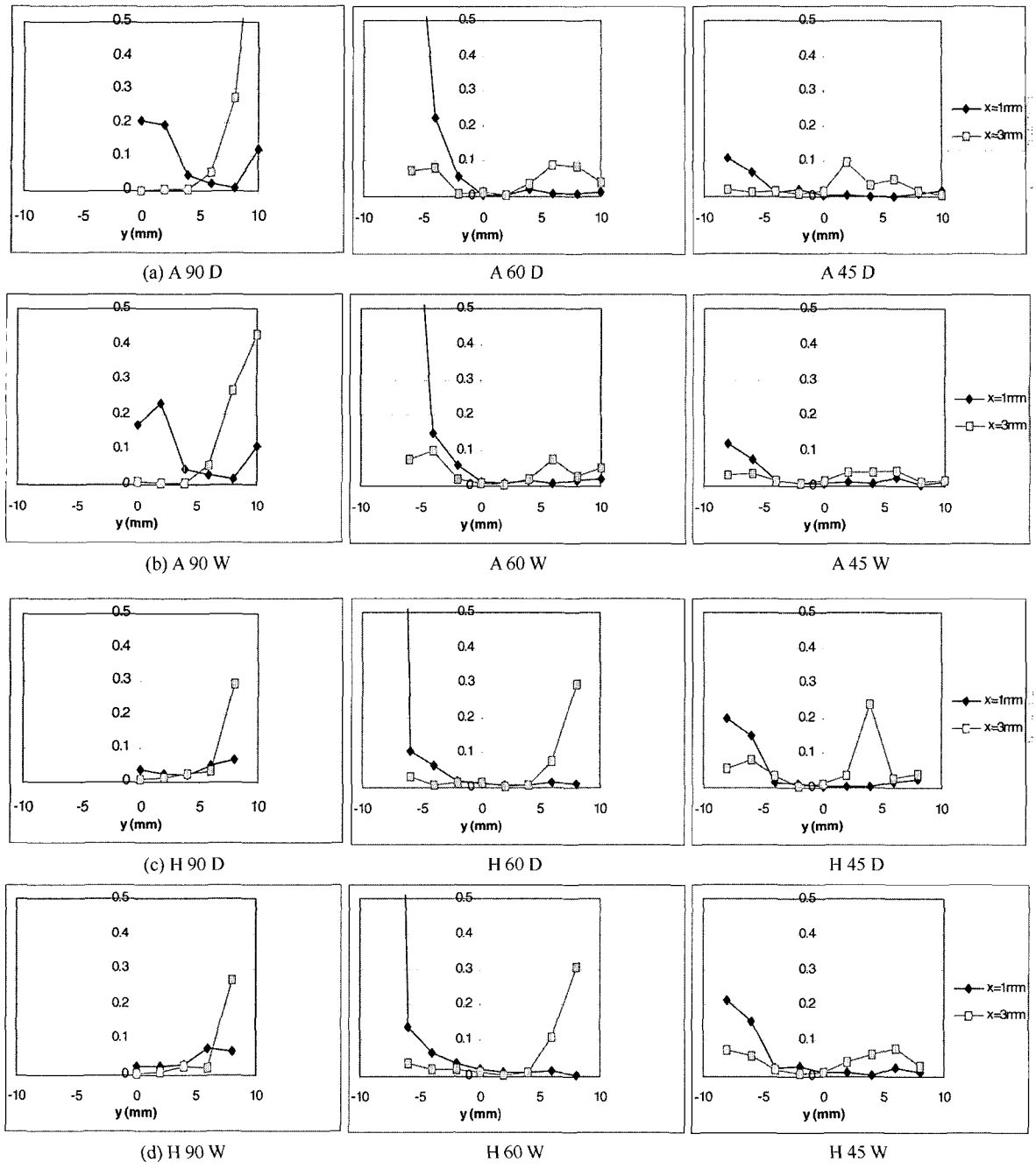

Figure 18. Time averaged PDI results: We_2/We.

angle is larger than the downhill side. In addition, the spray in the uphill side does not have enough space to develop a larger re-circulation zone so that more droplets impinge on the surface and produce higher n_2/n_1 ratio. The n_2/n_1 values for the wet surface cases are slightly higher than those in the dry surfaces due to more splashing effect. It is also interesting to note that the ratio is very high at y = −7 mm at the lower layer. Comparing Figure 16(a) and 16(b) with 16(c) and 16(d), the temperature dependence is obvious in the normal impingement cases, in which the inner peak is pushed out from y = 2 mm to y = 6 mm due to more vapor content in the spray center.

Figure 17 shows the 15-ms-averaged We_1, which is an indication of the breakup potential of the pre-impingement droplets. In all cases, the averaged We_1 is less than

20, which is much lower than the 400 range observed in single droplet measurement. The high chamber pressure also significantly reduces the droplet velocity. Comparing the results at two wall distances (x = 1 and 3 mm), We_1 is generally higher at distance further away from the wall, which is consistent with the time-resolved results shown in Figure 11. Another observation is that for heated cases, We_1 is higher around the center. This is an interesting fact considering n_2/n_1 is low around the center for the same cases, indicating that the stagnation flow field is stronger for heated cases.

Figure 18 shows the ratio, We_2/We_1, of the average Weber numbers. For most cases, the ratio is less than 0.5, and is higher at the edge of the spray, especially for q=60° impingement case. Similar to the trends observed in n_2/n_1 measurements: The ratio is highest at x=1 mm in the uphill side, and the temperature effect is more pronounced at normal impingement cases.

5. CONCLUSION

High-speed laser-sheet macroscopic visualization, wetted footprints, shadowgraph visualization, and PDI measurement techniques are used to characterize the fundamental impingement processes for a narrow-cone swirl-type DI gasoline injector. Two temperatures, two impingement surface conditions, and three impact angles are tested. The results provide valuable insights into the complex spray impingement processes. They are also useful for validation of CFD simulation. The results are summarized as follows:

(1) High-speed Macroscopic Visualization
Spray penetration speed shows a minor change, while spray width observed using the Mie scattering at elevated temperature conditions is reduced by approximately 10% from that under unheated cases due to droplet vaporization at the spray peripheral. Obvious upward spray vortex inside the spray is not clear due to the narrow cone spray structure, but faster evaporation is obvious at elevated temperature conditions.

(2) Shadowgraph Visualization
Evaporation of the spray is observed immediately after the impingement for heated and unheated conditions. Wet surface evaporation is more active, especially at elevated temperature conditions. It also shows splashing effect at the edge of the spray resulting from the splashing of the existing fuel film by impinging spray. Horizontal vapor phase propagation is approximately 10–20% faster at elevated temperature conditions, while vertical propagation does not show significant difference. Decrease of the impact angle promotes the spray plume to slide along the surface, resulting in longer horizontal vapor phase propagation.

(3) Wetted Footprints
The reduced width of the wetted footprints at oblique impact angle cases shows that there is significant variation in liquid fuel film formation and movement with respect to impingement angle. Only a few large sac spray droplets are visible due to the short injection duration.

(4) PDI Measurement
Effect of time, temperature, and impact angle on the wetting regime was tested using time-solved and timeaveraged analysis. The overall bulk motions of the spray plume and its spatial position at a given time are basically unaffected until a few millimeters before impacting the wall. Compared to the free spray measurement, wall impingement makes the distribution of the velocity component wider in the spray tails.

Only the spray front contains droplets having large enough momentum to break-up and splash from the surface. Most spray tails contain small droplets with Weber number below the splash threshold, which will either stick or spread along in the wall plume. However, Weber numbers of different droplets in one spray vary significantly according to their impingement locations, the surface temperatures.

As the impact angle decreases, both We_1 and We_2 decrease as well as the number of upward-bound droplets. Therefore, more spray droplets are reflected by the wall rather than impinging on the wall. High temperature affects the impinging spray patterns the most at normal impact angle condition. The effect of preexisting fuel film on the impinging spray is small for the cases tested, but increase the ratio of rebounded small droplets.

Droplet Weber number distributions are very sensitive to the impact angle and location. In most cases, the time-averaged We_1 tested is less than 20 with 15 ms after SOI. The rebound ratio, n_2/n_1, is generally less than 0.5, and is generally higher at outside than inside, and at uphill side than downhill side. The Weber number ratio We_2/We_1 tracts n_2/n_1 ratio very closely and is mostly low around the stagnation point, where We_1 is higher, indicating that the droplets away from impact stagnation point are mostly entrained airborne droplets. For oblique impingement cases, more rebound and splashed droplets are observed in the uphill side.

ACKNOWLEDGEMENT–The partial support from US TARDEC through the subcontract from the University of Michigan Automotive Research Center is gratefully acknowledged. The discussion with Dr. David L. Harrington of General Motor is very much appreciated.

REFERENCES

Bai, C. and Gosman, A. D. (1995). Development of methodology for spray impingement simulation. *SAE Paper No.* 950283.

Bai, C. and Gosman, A. D. (1996). Mathematical modeling of wall films formed by impinging sprays. *SAE Paper No.* 960626.

Habchi, C., Foucart, H. and Baritaud, T. (1999). Influence of the Wall temperature on the mixture preparation in di gasoline engines. *Oil & Gas Science and Technology Review, IFP*, **54, 2,** 211–222.

Han, Z., Xu, Z. and Trigui, N. (2000). Spray/Wall interaction models for multidimensional engine simulation. *Int. J. of Engine Research* **1, 1,** 127–146.

Li, J., Matthews, R. D., Stanglmaier, R. H., Roberts, C. E. and Anderson, R. W. (1999). Further experiments on the effects of in-cylinder wall wetting on HC emissions from direct-injection gasoline Engines. *SAE Paper No.* 1999-01-3661.

Mundo, C., Sommerfeld, M. and Tropea, C. (1994). Experimental studies of the deposition and splashing of small liquid droplets impinging on a flat surface. *ICLASS-94*, Rouen, France, July 1994.

Naber, J. and Reitz, R. D. (1988). Modeling engine spray/ wall impingement. *SAE Paper No.* 880107.

Nagaoka, M., Kawazoe, H. and Nomura, N. (1994). Modeling fuel spray impingement on a hot wall for gasoline engines. *SAE Paper No.* 940525.

Nishida, K., Min, J., Yoshida, H. and Hiroyasu, H. (1990). Computed tomographic study on the internal structure of a diesel spray impinging on a flat wall. *JSME International Journal* **57, 537,** 362–368.

Obert, E. F. (1973). *Internal Combustion Engines and Air Pollution.* Harper & Row. New York.

Park, J., Xie, X., Im, K.-S., Kim, H. and Lai, M.-C. (1999). Characteristics of direct injection gasoline spray wall impingement at elevated temperature conditions. *SAE Paper No.* 1999-01-3772.

Plackmann, J. D., Kim, J. and Ghandhi, J. B. (1998). The effects of mixture stratification on combustion in a constant-volume combustion vessel. *SAE Paper No.* 980159.

Senda, J., Ohnishi, M., Takahashi, T., Fujimoto, H., Utsunomiya, A. and Wakatabe, M. (1998). Measurement and modeling on wall wetted fuel film profile and mixture preparation in intake manifold for SI engine. *SAE Paper No.* 1998-01-0798.

Senecal, P. K., Stanton, D. W., Reitz, R. D. and Rutland, C. J. (1998). Modeling the effects of lift and drag forces on liquid drops in impinging sprays. *The 11th Annual Conference on Liquid Atomization and Spray Systems, ILASS-America*, May 17–20, 1998, Sacramento, California.

Stanglmaier, R. H., Li, J. and Matthews, R. D. (1999). The effect of in-cylinder wall wetting location on the HC emissions from SI engines. *SAE Paper No.* 1999-01-0502.

Stanton, D. W. and Rutland, C. J., Modeling fuel film formation and wall interaction in diesel engines. *SAE Paper No.* 960628.

Stevens, E. and Steeper, R. (2001). Piston wetting in an optical DISI engine: fuel films, poolfires, and soot generation. *SAE Paper No.* 2001-01-1203.

Wirth, M., Piock, W. F., Fraidl, G. K., Schoeggl, P. and Winklhofer, E. (1998). Gasoline DI engines: the complete system approach by interaction of advanced development tools. *SAE Paper No.* 980492.

Yoo, J.-H., Kim, S.-K., Zhao, F. Q., Lai, M. C. and Lee, K. S. (1998). Visualization of direct-injection gasoline spray and wall-impingement inside a motoring engine. *SAE Paper No.* 982702.

Zhao, F.-Q., Lai, M.-C. and Harrington, D. (1995). The spray characteristics of automotive port injection-a critical review. *J. Fuels & Lubricants* **104, 3,** 399–432, *SAE Paper No.* 950506.

Zhao, F.-Q., Lai, M.-C. and Harrington, D. L. (1999). Mixture dynamics and combustion control strategies in spark-ignited direct injection gasoline engines. *Prog. in Energy and Comb. Sci.*, **25,** 437–562.

Zhao, F.-Q., Lai, M.-C. and Harrington, D. L. (1997). A Review of mixture preparation and combustion control strategies in spark-ignited direct injection gasoline engines. *J. Engine* **106, 3,** 861–904, *SAE Paper No.* 970627.

Zulo, J. R. and Chigier N. (1991). Impinging diesel spray dynamics. *Atomization and Sprays*, **1,** 303–318.